Transmembrane Domain of Myelin Protein Zero Can Form Dimers: Possible Implications for Myelin Construction†

Megan L. Plotkowski,‡ Sanguk Kim,§ Martin L. Phillips,‡ Anthony W. Partridge,|| Charles M. Deber,|| and James U. Bowie*,‡

Department of Chemistry and Biochemistry, Molecular Biology Institute, and University of California at Los Angeles−U.S. Department of Energy Institute for Genomics and Proteomics, University of California, Los Angeles, 611 Charles E. Young Drive East, Los Angeles, California 90095-1570, Department of Life Science, POSTECH, Pohang, Kyungbuk 790-784, Korea, Division of Molecular Structure and Function, Research Institute, Hospital for Sick Children, Toronto M5G 1X8, Ontario, Canada, and Department of Biochemistry, University of Toronto, Toronto M5S 1A8, Ontario, Canada

Received May 31, 2007; Revised Manuscript Received August 17, 2007

ABSTRACT: Myelin protein zero (MPZ) is the major integral membrane protein of peripheral nerve myelin in higher vertebrates, mediating homoadhesion of the multiple, spiraling wraps of the myelin sheath. Previous studies have shown that full-length MPZ can form dimers and tetramers, and biochemical studies on the extracellular domain (ECD) indicate that it can form a tetramer, albeit very weakly. On the basis of cross-linking studies and equilibrium sedimentation of a transmembrane (TM) domain peptide (MPZ-TM), we find that the MPZ-TM can form homodimers. We further characterized the dimer by measuring the effects of alanine and leucine substitutions on the ability of the TM to dimerize in *Escherichia coli* membranes. Our results indicate that the primary packing interface for the MPZ TM homodimer is a glycine zipper (GxxxGxxxG) motif. We also find that the G134R mutation, which lies within the glycine zipper packing interface and causes Charcot−Marie−Tooth disease type 1B, severely inhibits dimerization, suggesting that dimerization of the TM domain may be important for the normal functioning of MPZ. By combining our new results with prior work, we suggest a new model for an MPZ lattice that may form during the construction of myelin.

Myelin protein zero (MPZ)[1] is an integral membrane glycoprotein (*1*) expressed in peripheral nerve cells (*2*, *3*) that comprises over 80% of the total protein content of the mature myelin sheath (*4*). MPZ functions as an adhesion molecule in compact myelin, where it is thought to stabilize and adhere to adjacent layers of myelin membranes through homotypic interactions (*3*, *5*−*7*). Point mutations in the gene encoding MPZ result in a wide variety of peripheral nervous system diseases that are classified as Charcot−Marie−Tooth disease type 1B, Dejerine−Sottas syndrome, and congenital hypomyelination (*8*−*10*). It is hypothesized that some of these mutations cause changes that may affect the tertiary and quaternary structures of MPZ, contributing to demyelination, reduced motor nerve conduction velocities, and other characteristic pathological features (*11*−*15*).

Human MPZ is composed of 219 residues that can be divided into three distinct domains: an N-terminal extracellular domain (ECD) (residues 1−124) that belongs to the immunoglobulin superfamily of proteins (*3*, *16*), a single transmembrane (TM) segment (residues 125−151), and a C-terminal cytoplasmic domain (residues 152−219).

A crystal structure of the ECD from rat MPZ has been reported and possible tetramers were observed in the crystal (*17*). Based on the packing arrangement of tetramers in the rat ECD crystal structure, a model was proposed for how the tetramers could assemble between apposing membranes of the myelin sheath (*17*). Tetramerization of the ECD could also be observed in solution but only at high concentrations (>1 mM) (*17*). Nevertheless, it is possible that tetramers could be stabilized by tethering to the membrane, which would reduce the entropy cost of oligomerization relative to solution conditions.

In spite of the extensive studies on the ECD, there is little consensus on the inherent oligomeric state of full-length MPZ. X-ray scattering analysis of whole MPZ isolated from bovine peripheral nervous system membranes indicated that full-length protein can form tetrameric assemblies in SDS micelles (*18*). On the other hand, protein extracts from human peripheral nerve tissue revealed the presence of SDS-resistant MPZ dimers (*19*). Finally, studies on full-length MPZ isolated from *Xenopus* myelin membranes revealed the presence of both dimers and tetramers on SDS−PAGE (*20*).

† Supported, in part, by NIH Grant RO1 GM063919 to J.U.B. and a grant to C.M.D. from the Canadian Institutes of Health Research (CIHR). A.W.P. held a CIHR doctoral research fellowship.

* To whom correspondence should be addressed: e-mail bowie@mbi.ucla.edu.
‡ University of California at Los Angeles.
§ POSTECH.
|| Hospital for Sick Children and University of Toronto.

[1] Abbreviations: BS^3, bis(sulfosuccinimidyl) suberate; CAT, chloramphenicol acetyltransferase; CMT1B, Charcot−Marie−Tooth disease type 1B; DMSO, dimethyl sulfoxide; DSS, Dejerine−Sottas syndrome; ECD, extracellular domain; EDTA, ethylenediaminetetraacetic acid; GpA, glycophorin A; MALDI-TOF, matrix-assisted laser desorption ionization time-of-flight; MBP, maltose binding protein; MC, Monte Carlo; MPZ, myelin protein zero; TM, transmembrane; WT, wild type.

10.1021/bi701066h CCC: $37.00
Published on Web 10/04/2007

Given the relatively weak tetramerization of the ECD, the oligomerization observed in SDS suggests the involvement of other regions. We previously noted a GxxxGxxxG sequence motif in MPZ, called a glycine zipper, which is strongly associated with TM helix oligomerization (*21*). The glycine zipper places three glycines on one side of a TM helix, forming a favorable interface for TM helix packing. Indeed, all glycine zippers observed in known membrane protein structures are directly involved in helix packing. Thus, the presence of a glycine zipper in MPZ is a strong indication that the TM segment could be involved in oligomerization. Moreover, the only two known phenotypic mutants that lie within the MPZ TM domain are both glycine to arginine substitutions within the glycine zipper, an additional indicator that the glycine zipper in wild-type MPZ may be participating in helix−helix packing.

Here we present experimental evidence that the MPZ TM domain forms stable dimers that are mediated by the glycine zipper motif. Combining these findings with previous results indicating that the ECD can form tetramers, we propose a new model for the MPZ adhesion structure in which dimers of tetramers form a complementary lattice that bonds adjacent layers of the myelin sheath.

EXPERIMENTAL PROCEDURES

Vectors and Constructs. The TOXCAT vectors pccKAN, (containing no TM domain), pccGpAWT (containing WT GpA), and pccGpA83I (containing a monomeric GpA mutant) were described previously (*22*). A new vector encoding the wild-type MPZ TM segment, pccMPZ-WT, was prepared by replacing the *Nhe*I/*Bam*HI fragment of pccGpAWT encoding the TM region, with a synthetic DNA oligonucleotide cassette coding for the MPZ TM domain. The sequences of the oligos used to make the wild-type MPZ cassette are as follows: forward strand, 5′-CTAGCTACGGTGTTGTTCTGGGTGCTGTTATCGGTGGTGTTCTGGGTGTTGTTCTGCTGCTGCTGCTGTTCTACGTTGTTGG; reverse strand, 5′-GATCCCAACAACGTAGAACAGCAGCAGCAGCAGCAGAACAACACCCAGAACACCACCGATAACAGCACCCAGAACAACACCGTAG. The resulting amino acid sequence is RASYGVVLGAVIGGVLGVVLLLLLLFYVVGIL.

Site-Directed Mutagenesis. Site-directed mutagenesis was performed on pccMPZ-WT using the Quik Change Site-Directed Mutagenesis kit (Stratagene, La Jolla, CA). Mutations were confirmed by sequencing of the TM encoding regions.

Expression of ToxR′(TM)MBP Chimeras. Plasmids encoding all of the ToxR(TM)MBP constructs were transformed into NT326 cells and MM39 cells (kindly provided by Donald Engelman) and plated onto Luria−Bertani (LB) plates (containing 50 μg/mL carbenicillin). Colonies were inoculated into liquid LB broth (with 50 μg/mL carbenicillin) and grown overnight, and in the morning, glycerol stocks were made at and stored at −80 °C. Growth and expression of each construct was then performed via methods published by Sulistijo et al. (*23*). Liquid LB cultures (2 mL each, containing 50 μg/mL carbenicillin) were inoculated with glycerol stocks, grown overnight, and in the morning diluted at least 40-fold into fresh 2 mL cultures. These cultures were grown to OD_{420} of approximately 1.0 and diluted 40-fold again into fresh, 6 mL cultures. The 6 mL cultures were again grown to OD_{420} of approximately 1.0. Cells were collected by centrifugation and washed with 0.5 mL of lysis buffer (25 mM Tris-HCl pH 8.0, and 2 mM EDTA). The pellet was then resuspended in 1 mL of lysis buffer and lysed by freeze−thaw four times. After removal of an aliquot (100 μL) for western blot analysis, the remaining lysate was cleared by centrifugation at 13 000*g* for 20 min and stored on ice until the CAT assays were performed. Lysate concentrations were normalized by assaying total protein (Bio-Rad).

Spectrophotometric CAT Assays. A modification of the assays by Sulistijo et al. (*23*) and Shaw (*24*) was used to detect chloramphenicol acetyltransferase (CAT) activity in cell lysates. This method monitors the release of coenzyme A upon transfer of an acetyl group from acetyl-CoA to chloramphenicol, by monitoring the color change that occurs at 412 nm upon reaction of the free thiol of CoA-SH with 5,5′-dithiobis(2-nitrobenzoic acid). Aliquots (10 μL) of each cell lysate were added to the wells of a 96-well plate, and 200 μL of an assay mix containing 0.1 mM acetyl-CoA, 0.4 mg/mL 5,5′-dithiobis(2-nitrobenzoic acid), 2.5 mM chloramphenicol, and 0.1 M Tris-HCl, pH 7.8, was then added to start the reaction. The absorbance at 412 nm was recorded in the linear range. Each lysate was assayed in triplicate; the three slopes were averaged and then normalized by total protein concentration. All kinetics traces were recorded with a Molecular Devices Spectramax M5.

Western Blots. Cell lysates were mixed 1:1 with 2× SDS−PAGE sample buffer containing fresh β-mercaptoethanol, separated by electrophoresis on precast 4−20% gels (Novex), blotted onto poly(vinylidene difluoride) (PVDF) membrane, detected with an anti-MBP primary antibody (Zymed), and visualized with an anti-mouse IgG (whole molecule) horseradish peroxidase conjugate (Sigma) and enhanced chemiluminescence (ECL) reagents (Amersham Biosciences).

Maltose Complementation Assays. To confirm that constructs were inserting into the *E. coli* inner membrane in the proper orientation, the ability of cells expressing TOXCAT chimerae to grow on minimal medium with maltose as the only carbon source was tested. *E. coli* MM39 cells expressing TOXR′(TM)MBP constructs were inoculated into liquid minimal medium containing 0.4% glucose and grown overnight. In the morning, cells were harvested, washed in PBS, streaked onto M9 minimal medium plates (with 50 μg/mL carbenicillin) containing 0.04% maltose, and incubated for 2 days at 37 °C.

Chemical Cross-Linking. A time course of chemical cross-linking was performed to examine the oligomeric state of the TOXCAT constructs as well as the MPZ-TM peptide. To analyze the TOXCAT-MPZ constructs, glycerol stocks of MM39/pccMPZ cells were inoculated into 2 mL overnight cultures of LB liquid medium containing 50 μg/mL carbenicillin. Cultures were diluted 40-fold in the morning into 6 mL of LB medium (with 50 μg/mL carbenicillin) and grown to OD_{420} ~1.0. Aliquots (6 mL) of cells were collected by centrifugation and resuspended in 500 μL of fresh cross-linking buffer (150 mM NaCl and 50 mM sodium phosphate, pH 7.5). Freeze−thaw was performed four times to lyse the cells. The lysate was spun in a microcentrifuge at 13 000*g* for 10 min and the supernatant was discarded. The pellet

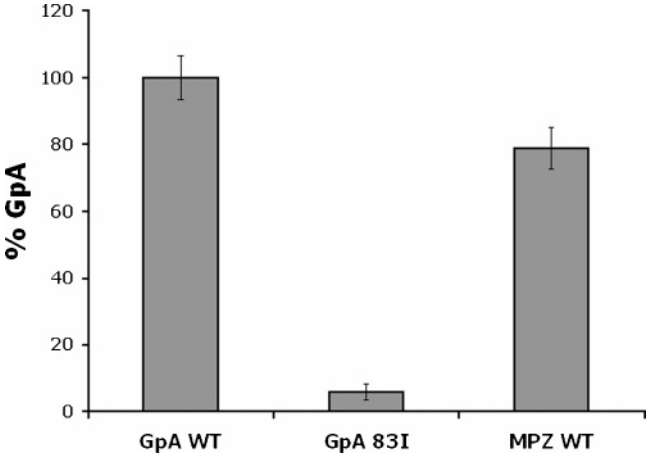

FIGURE 1: MPZ TM domain can oligomerize in *E. coli* membranes. Spectrophotometric CAT assays of TOXCAT constructs containing the TM domains of GpA, GpA 83I (a monomeric mutant), and MPZ are shown, normalized to the CAT activity of GpA. Each experiment was run in triplicate.

was resuspended in 500 μL of fresh cross-linking buffer containing 1% *n*-dodecyl β-D-maltopyranoside (DDM, Anatrace). Aliquots (40 μL) of this solution were transferred to 150 μL Eppendorf tubes and 10 μL of a 1.25 mM stock of bis(sulfosuccinimidyl) suberate (BS^3, Pierce) in DMSO was added for 0, 5, 10, 30, or 60 min at room temperature, for a total volume of 50 μL and a working concentration of 250 μM cross-linker. Reactions were quenched with 20 μL of 2× SDS−PAGE loading buffer containing 100 mM Tris, pH 8.5, and fresh β-mercaptoethanol. Samples were spun down at 13000*g* for 20 min to clear the lysates and subjected to electrophoresis on 4−20% Bis Tris gels (Novex) followed by western blotting.

The MPZ-TM peptide was cross-linked in a buffer containing 200 mM NaCl, 20 mM sodium phosphate, pH 7.0, and 1% (w/v) penta(ethylene glycol) monooctyl ether (C_8E_5, Sigma). Two different concentrations of peptide, 0.6 mg/mL (~140 μM) and 1.2 mg/mL (~280 μM), were cross-linked with three different concentrations of BS^3 (100, 250, and 500 μM). At the appropriate time points, samples were quenched with 100 mM Tris, pH 8.5, and analyzed by MALDI-TOF mass spectrometry. Under the conditions used, we saw dimer formation prior to the attachment of multiple cross-linkers, but multiple cross-linkers per peptide were seen with higher concentrations of cross-linker or if the reaction was left to proceed for long periods of time.

MALDI-TOF Mass Spectrometry. Peptide mass fingerprints were obtained of cross-linked peptide samples as well as non-cross-linked controls in the mass range of 2 000−50 000 Da. Samples were prepared according to the methods of Schey et al. (*25*). An aliquot (3 μL) of each sample was added to 7 μL of 99% formic acid (Sigma), followed by 2 μL of hexafluoroisopropanol (Sigma). These samples were then gently mixed in ratios of 1:3 and 1:7 in a saturated solution of sinapinic acid (Sigma) in 70% formic acid. An aliquot (1 μL) of each sample was placed onto a 100-well gold PerSeptive Biosystems plate and air-dried. Samples were analyzed on a linear (1 m) Applied Biosystems Voyager time-of-flight mass spectrometer with a nitrogen laser focused to a 100 μm^2 spot emitting 337 nm photons with a power density of 10 MW/cm^2. One thousand shots were collected per spectrum and data were analyzed with Voyager Software.

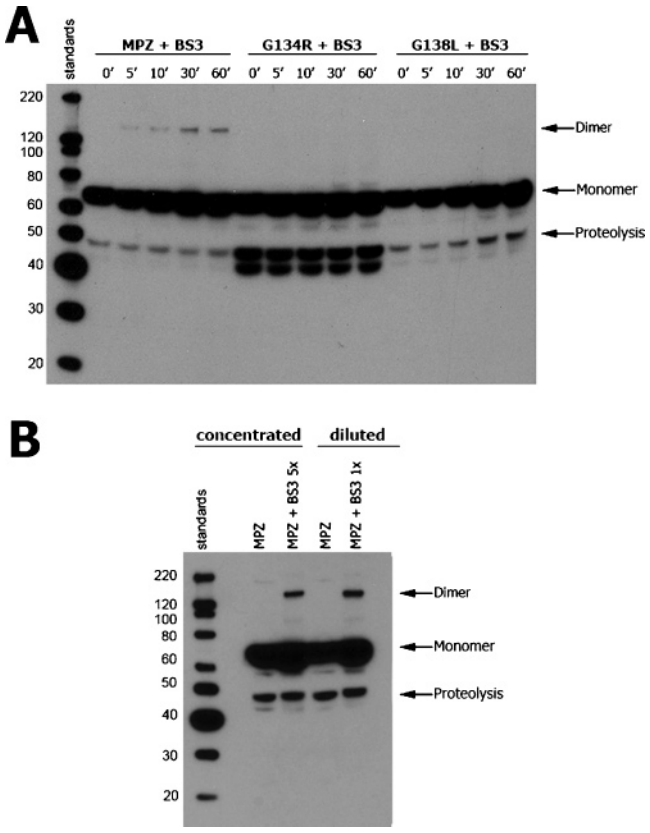

FIGURE 2: TOXCAT-MPZ construct can be cross-linked to a dimer. (A) Cells expressing WT TOXCAT-MPZ, or one of two different glycine zipper mutants (G134R and G138L), were cross-linked in 100 μM BS^3 over a time course of 1 h in DDM micelles. At the appropriate time points, the reactions were quenched and the fusion proteins were separated by SDS−PAGE and detected by western blotting with an anti-MBP antibody. (B) Rate of cross-linking, compared for concentrated and 5-fold diluted samples of cell lysates containing TOXCAT MPZ in 1% DDM. After 1 h of cross-linking in 250 μM BS^3, the samples were quenched and the concentrated sample was diluted 5-fold to approximately equalize the two concentrations. Arrows indicate the positions of the TOXCAT monomer as well as cross-linked dimer, and the bands below the 66 kDa TOXCAT monomer are assumed to be proteolytic breakdown products.

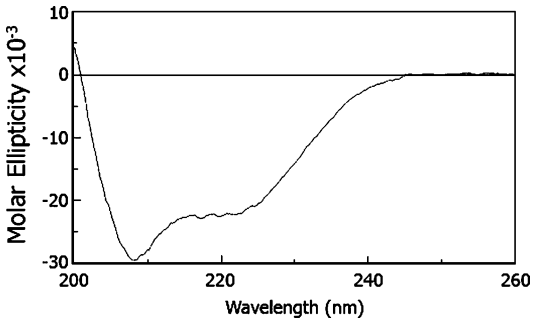

FIGURE 3: Circular dichroism confirms that the MPZ-TM peptide is α-helical. CD spectrum of 0.043 mg/mL peptide in a buffer containing 20 mM Tris pH 7.8, 20 mM NaCl, and 1% (w/v) C_8E_5 is shown.

Peptide Design and Synthesis. The hydrophobic MPZ-TM peptide was flanked with lysine residues to improve solubility (*26*). The sequence of the peptide is as follows: KKKKKKYGV-VLGAVIGGVLGVVLLLLLLFYVVRKKKKKK. The peptide was synthesized by CS BIO, and 5 mg of >96% pure peptide was recovered by HPLC and confirmed by mass spectroscopy.

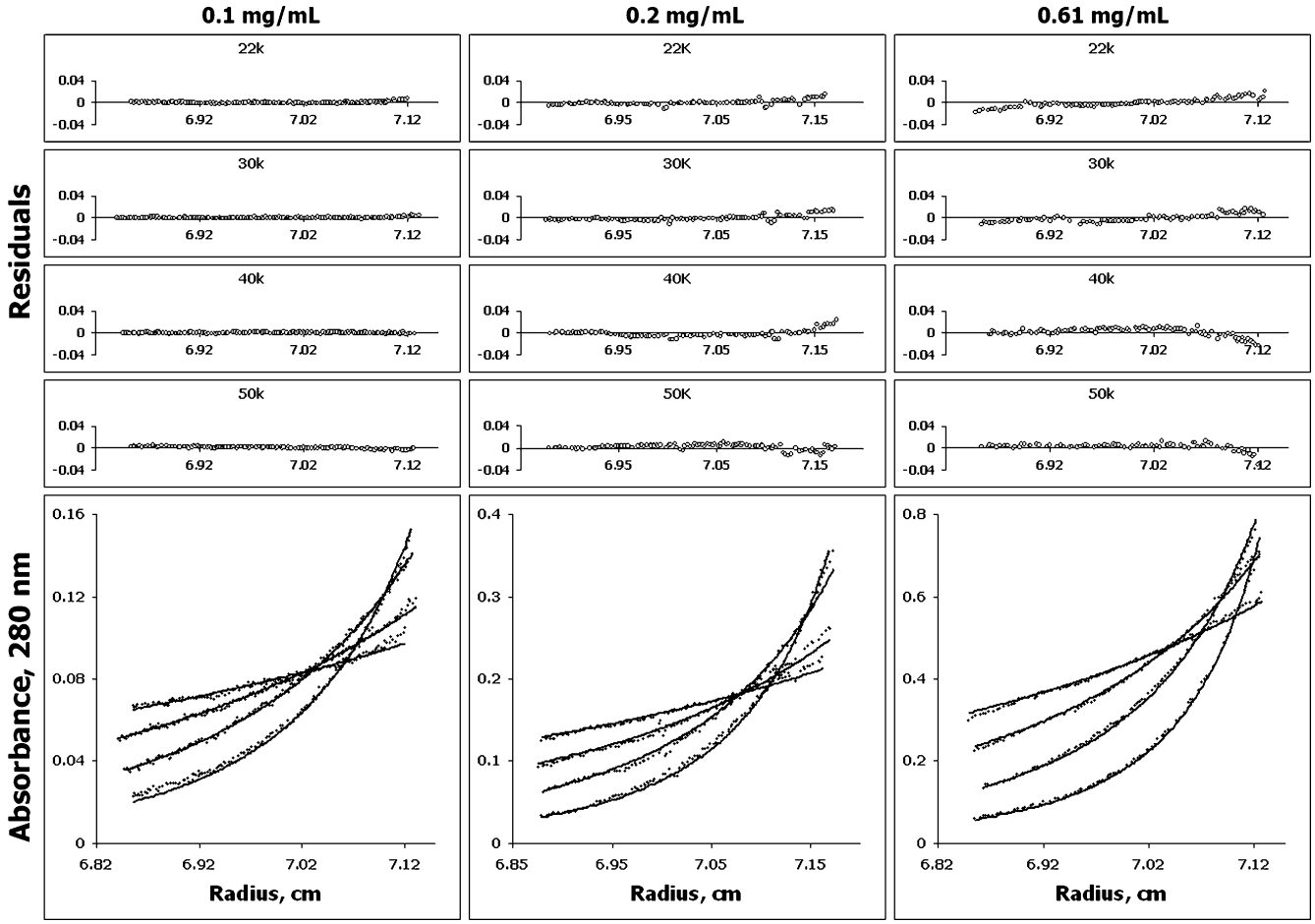

FIGURE 4: Sedimentation equilibrium is consistent with MPZ-TM peptide dimerization. (Upper panels) Equilibrium distribution data are shown for three concentrations of peptide (0.1, 0.2, and 0.61 mg/mL) and four different speeds (22 000, 30 000, 40 000, and 50 000 rpm) in a buffer containing 200 mM NaCl, 20 mM sodium phosphate, pH 7.0, and 1% (w/v) C_8E_5. (Lower panels) Data points for runs at each concentration are shown as black dots, and the best fits as determined by global analysis are illustrated as black lines. Residuals for each concentration of peptide at each speed are depicted in the four panels above each data set.

Circular Dichroism. Spectra were recorded on a Jasco J-715 spectrapolarimeter. The sample contained 0.043 mg/mL peptide in 20 mM Tris, pH 7.8, 20 mM NaCl, and 1% (w/v) C_8E_5. Data were analyzed by use of a secondary structure algorithm from Sreerama and Woody (*27*).

Analytical Ultracentrifugation. Sedimentation equilibrium profiles were measured at 22 000, 30 000, 40 000, and 50 000 rpm on samples with initial concentrations of 0.10, 0.20, 0.61, 0.94, 3.7, or 10.5 mg/mL. Sedimentation equilibrium runs were performed at 20 °C on a Beckman Optima XL-A analytical ultracentrifuge using absorption optics at 280 or 290 nm (for the 10.5 mg/mL run). Twelve-millimeter pathlength double sector cells were used, except for the 3.7 and 10.5 mg/mL runs, which used 3 mm centerpieces. All samples were in a buffer of 200 mM NaCl, 20 mM sodium phosphate, pH 7.0, and 1% (w/v) C_8E_5, a non-ionic detergent chosen because it has a hydrated density such that the contribution of bound detergent to the measured molecular weight is negligible (*28*). Scans were determined to be at equilibrium when consecutive scans at 4 h intervals were essentially identical, determined by examination of the residuals produced by subtracting one scan from the other. After a run, inverting the cells several times to mix the samples and rerunning them gave essentially the same absorbance distributions. The data were initially fitted with a nonlinear least-squares exponential fit for a single ideal species with Beckman Origin-based software (Version 3.01). To evaluate various models, Beckman global analysis software ("multifit" option) was used to analyze multiple scans simultaneously. The final analysis utilized 12 scans, the four speeds at the three lowest concentrations. A partial specific volume of 0.817 calculated from the amino acid composition and corrected to 20 °C was used (*29*, *30*).

Model Building. The modeling procedures for TM helix oligomerization have been described (*31*, *32*). Briefly, the TM domain sequence of MPZ was built into uniform α-helices having backbone torsion angles of $\phi = -65°$ and $\psi = -40°$. We used the backbone-dependent rotamer library program SCWRL (*33*) to choose the side-chain rotamers. Then, Monte Carlo (MC) minimizations were performed to produce a collection of well-packed structures. After the MC simulations, the helix-dimer structures were filtered to remove structures incompatible with the dimeric symmetry. We then clustered the remaining structures by Cα rms distances. The median model from the largest cluster was selected as our final predicted structure.

RESULTS

MPZ Wild-Type TM Oligomerizes in E. coli Membranes. To test whether the TM domain of MPZ can oligomerize, we used the TOXCAT assay (*22*). In the TOXCAT system,

the TM domain of interest is inserted as a fusion between the N-terminal transcriptional activator, ToxR, and a C-terminal maltose binding protein (MBP) that acts as a periplasmic reporter. ToxR is a transcriptional activator that binds to DNA as a dimer. As a result, transmembrane domain oligomerization can enhance DNA binding of ToxR and, in turn, the expression of transcripts under ToxR control. ToxR activates expression of the chloramphenicol acetyltransferase (CAT) gene, and the level of CAT expression can be correlated directly with TM helix affinity. The TOXCAT system has been widely used to study and characterize TM helix association (*22*, *23*, *34*, *35*).

The results of the TOXCAT test indicate that MPZ TM domain can oligomerize strongly in membranes. As shown in Figure 1, the MPZ TM induces similar CAT activity to glycophorin A (GpA), a strongly dimerizing TM domain (*22*, *28*, *36*). Western blots of whole-cell lysates indicated that all of the constructs were expressed at equal levels (data not shown).

Chemical Cross-Linking Reveals That ToxR(MPZ WT)-MBP Can Form Dimers. To further investigate the oligomeric state of the TOXCAT chimeras, we attempted to chemically cross-link three different TOXCAT constructs (wild-type MPZ, G134R, and G138L). As discussed below, the G134R and G138L mutants do not oligomerize in the TOXCAT assay. Chemical cross-linking with BS^3 (11.4 Å spacer length) was performed in 1% DDM during a time course of 1 h. At the appropriate times, the reactions were quenched and then separated by SDS−PAGE. As shown in Figure 2A, after 60 min of exposure to BS^3, the wild-type MPZ TM domain is cross-linked to a dimer. There was no detectable cross-linking with either of the two mutants, suggesting that they are not in close proximity in DDM micelles and also indicating that little intermolecular cross-linking occurs. To verify that the observed cross-linking is specific to the dimer and not an intermolecular reaction between monomers, the rate of cross-linking was compared for concentrated and 5-fold diluted samples (Figure 2B). The fraction of cross-linked dimer did not decrease upon dilution as would be expected if the cross-linking were dominated by intermolecular reactions. As shown in Figure 2B, the protein cross-links overwhelmingly to dimers, but when overexposed, the western blot does show a faint, higher molecular weight band that could either be a higher order oligomer or possibly nonspecific cross-linking artifacts. Like the TOXCAT results, the cross-linking experiments indicate that the MPZ TM domain can drive oligomerization.

Soluble MPZ TM Peptide Can Form Dimers. The results discussed above indicate that MPZ TM domain can oligomerize at least as dimers. As the cross-linking experiments were performed on a large fusion protein, however, it is possible that attached domains prevented higher order oligomerization. We therefore sought to test the oligomeric state of the MPZ TM alone.

We synthesized an MPZ TM peptide (MPZ-TM) with additional flanking lysine residues to aid with solublization (*26*). The circular dichroic spectrum of MPZ-TM in 1% C_8E_5, shown in Figure 3, is consistent with a helical content of about 65% and about 35% random coil. This is exactly what we would expect for a helical MPZ-TM peptide since the flanking sequence corresponds to 35% of the total residues.

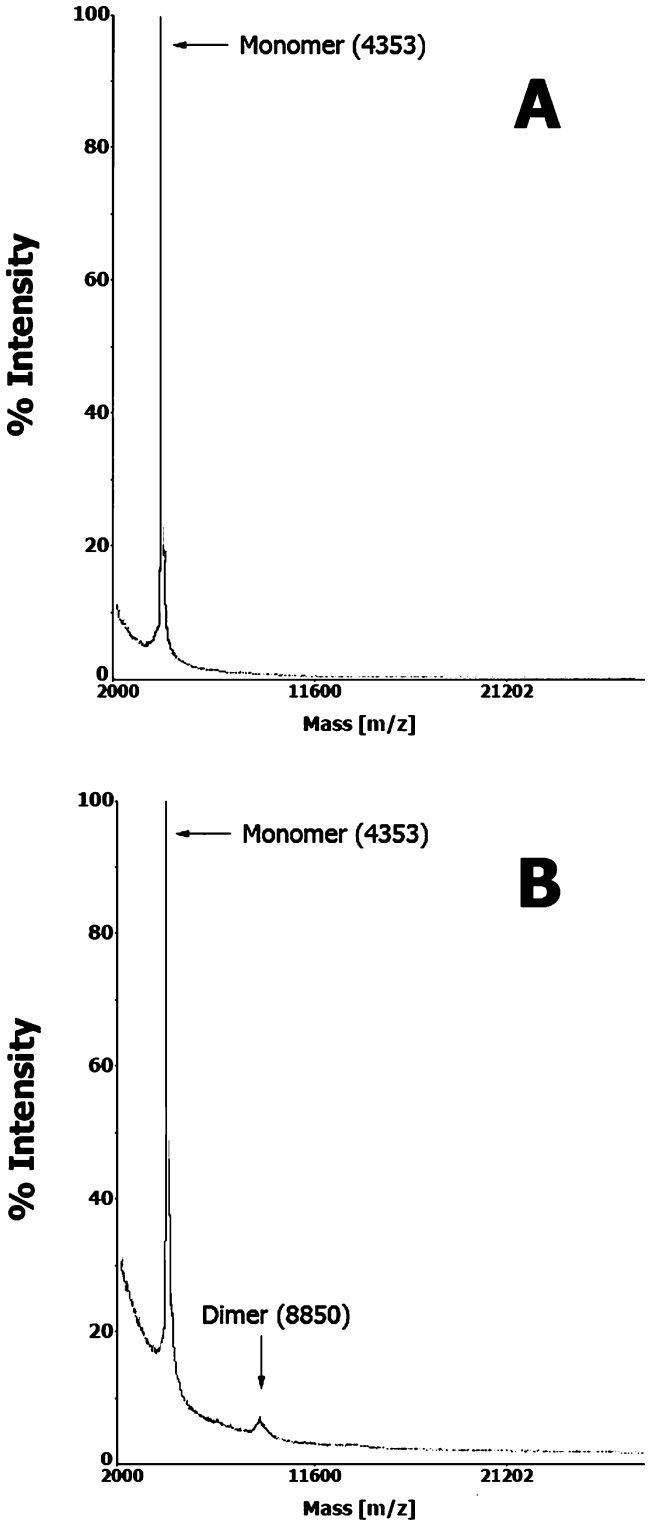

FIGURE 5: Chemical cross-linking of the MPZ-TM peptide followed by MALDI-TOF mass spectrometry is consistent with preferential dimerization of the MPZ-TM peptide. MPZ-TM peptide was cross-linked in the same buffer conditions used for equilibrium sedimentation runs. Peptide (0.6 mg/mL) was cross-linked in 250 μM BS^3 over a 1 h time course, followed by MALDI-TOF. (A) Spectrum for the peptide at time zero. (B) Typical mass spectrum from an experiment with a cross-linking time of 1 h. For all concentrations of peptide and cross-linker tested, nothing larger than a dimer was ever detected until the reaction was allowed to proceed for longer than 1 h.

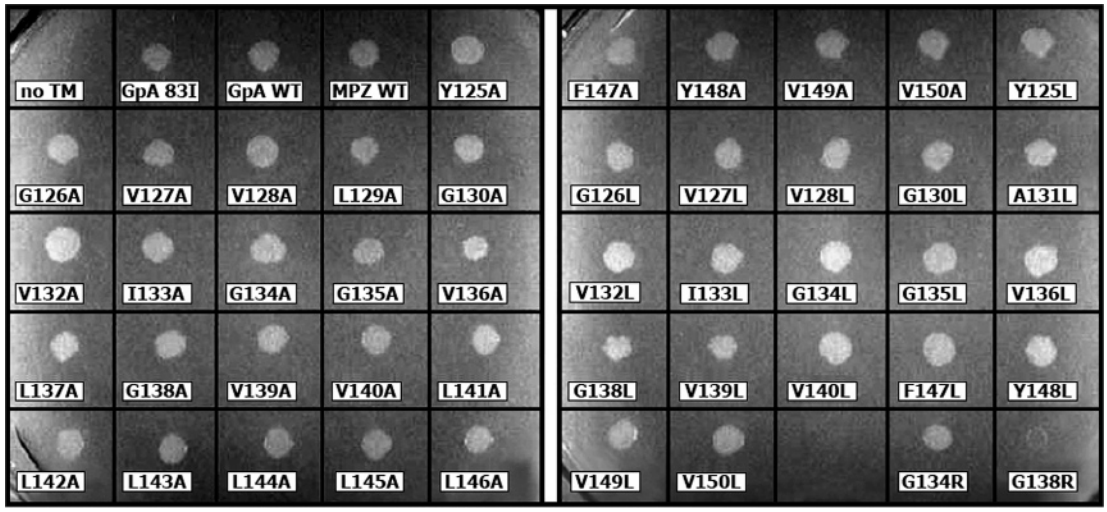

FIGURE 6: Maltose complementation assays for all TOXCAT constructs. MM39 cells expressing TOXCAT chimerae are tested for growth in minimal medium with maltose as the only carbon source. Positive controls for growth in this assay are GpA WT and GpA 83I. A construct containing no TM domain provides a negative control. MPZ WT, each point mutation in the alanine/leucine scan, and the two disease-related mutants are all tested for growth. Results indicate that all constructs are expressed and inserted properly in the *E. coli* inner membrane except for G138R, one of the two disease-related mutants (lower right).

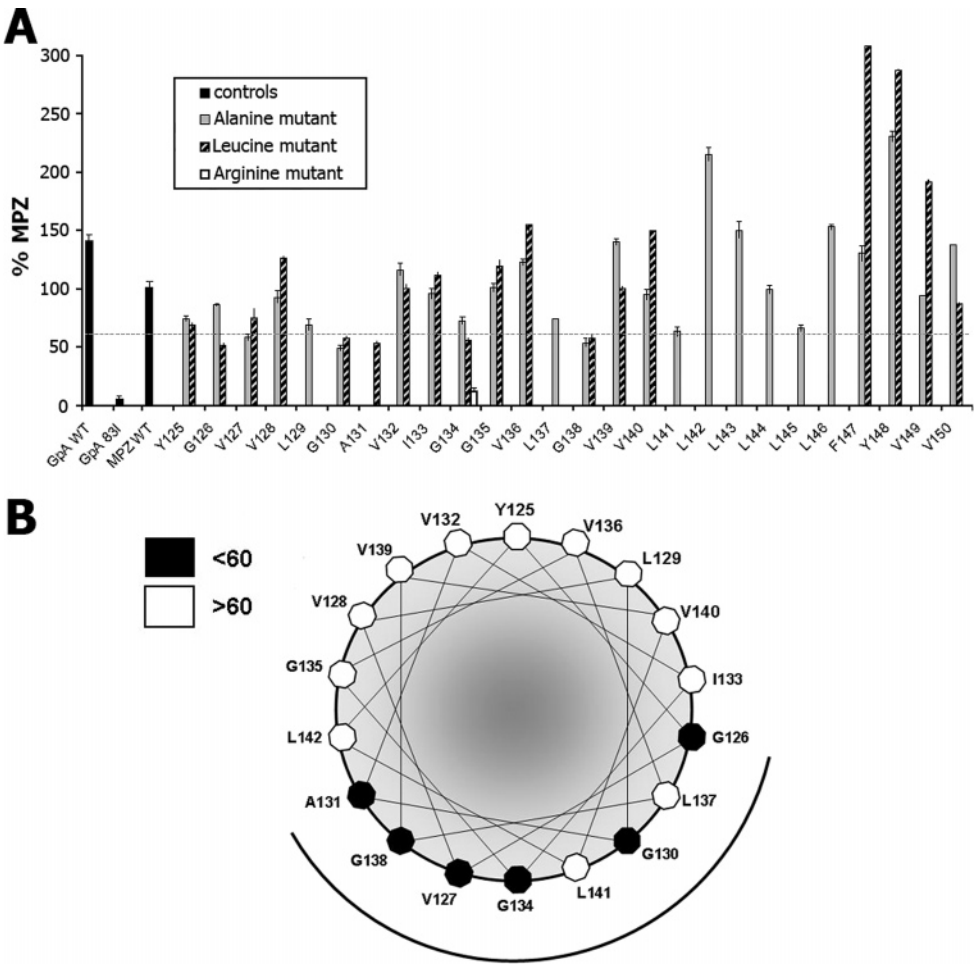

FIGURE 7: Spectrophotometric CAT assays of each point mutation in the MPZ TM reveal key residues involved in dimerization and the primary interaction surface. (A) CAT assays of the various TOXCAT constructs. Solid bars, controls (GpA WT, GpA 83I, and MPZ WT); gray bars, alanine mutants; striped bars, leucine mutants; open white bar, arginine mutant. The activity of each mutant is normalized to MPZ WT, which is set at 100% activity. Each experiment was run in triplicate. A dashed, gray line is drawn at the level of 60% activity relative to wild-type MPZ TM. (B) Relative effects of point mutations on residues 125−142 of MPZ TM on CAT activity are shown in a helical wheel plot. The most deleterious effects of either the Ala or Leu substitution on CAT activity were taken as an indicator of potential involvement in dimerization. Black indicates positions of mutants (either Ala or Leu) that showed less than 60% of activity relative to MPZ WT. White indicates mutations where both Ala and Leu substitutions maintained 60% or higher activity relative to MPZ. The black semicircular line indicates the most likely interface for dimerization.

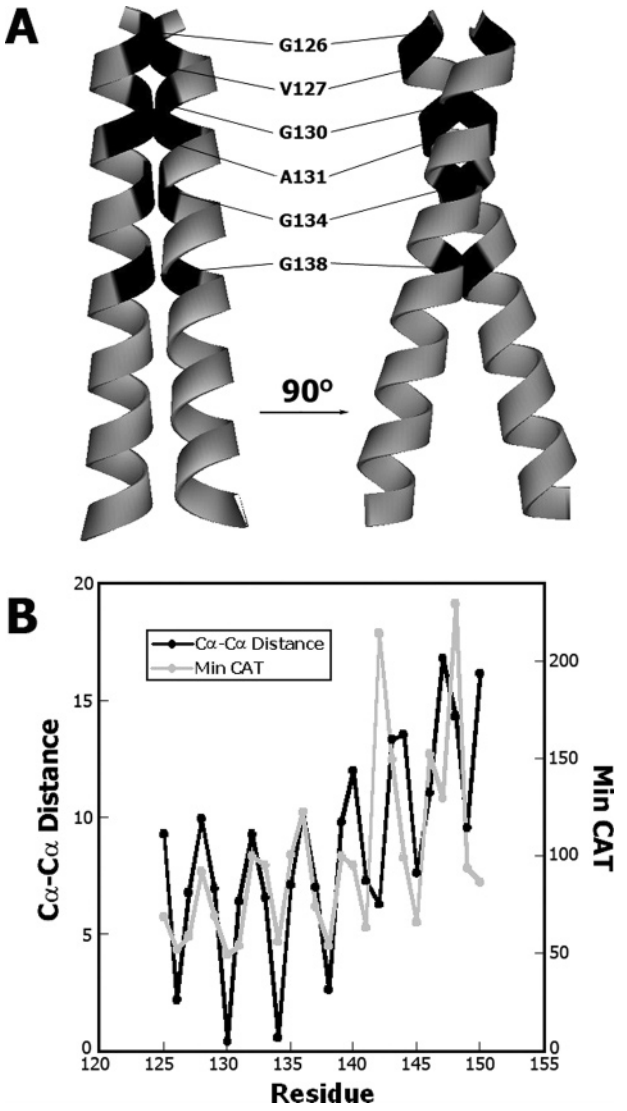

FIGURE 8: Computational model of MPZ TM dimer. (A) Model structure. Residues that showed a knockdown of at least 60% activity relative to MPZ WT in CAT assays are shown in black and tend to lie at the interface of the dimer, indicating good correlation between model and experimental results. The model structure on the left is rotated 90° to produce the model on the right. (B) Correlation between CAT activity assays and the Cα−Cα distances across the dimer interface. Graph shows an overlay of two separate sets of data: (black) distances between the α-carbons between each residue in the computational model; (gray) most extreme knockdown of CAT activity (via Ala or Leu mutations) for each residue in the TM as obtained experimentally.

To determine the oligomeric state of the MPZ-TM peptide, we employed equilibrium analytical ultracentrifugation. As the C_8E_5 detergent has the same density as water, the sedimentation behavior is dependent on the mass of the peptide oligomer. Sedimentation equilibrium distributions were initially analyzed with a single-exponential fit for a single ideal species. The weight-average molecular weights determined were speed-dependent, decreasing with increasing speed, suggestive of molecular weight heterogeneity, a result that was also suggested by the nonrandom nature of the residuals to the fits. The molecular weights were also concentration-dependent, increasing with increasing concentration, indicating an associating system. Sedimentation equilibrium analysis of the system was complicated by aggregation of the peptide at very high peptide concentrations. For example, at 10.5 mg/mL and 22 000 rpm, the weight-average molecular weight was 40 100 Da, corresponding to greater than a 9-mer on average. To avoid complications from nonspecific high molecular weight aggregation, the three lower concentrations (0.1, 0.2, and 0.61 mg/mL) were used to analyze the association behavior of the smaller, highest affinity complexes. The weight-average molecular weights varied from 9080 Da (for the highest concentration and lowest speed) to 5251 Da (for the lowest concentration and highest speed). As the molecular weight of the peptide determined by mass spectroscopy was 4353, these correspond to 2.1 to 1.2 times the molecular weight of the monomer. Global analysis of 12 conditions (three concentrations at four speeds) indicated that the system could be best fit by a monomer−dimer equilibrium plus an additional, higher molecular weight term: either monomer−trimer or monomer−tetramer (which is equivalent to a monomer−dimer, dimer−tetramer equilibrium). Floating both the monomer−dimer and monomer−tetramer equilibrium constants gave K_d values of 96 μM for the monomer−dimer equilibrium and 170 μM for the dimer−tetramer equilibrium (Figure 4). Thus, the peptide appears to favor association as a dimer but is prone to higher order aggregation, like many hydrophobic peptides.

Peptide aggregation at higher concentrations left some ambiguity in the results of our equilibrium sedimentation runs. We therefore performed a cross-linking experiment as an additional check on the predominant oligomeric state of the peptide in detergent micelles. We again employed the amine-reactive cross-linker BS^3 (11.4 Å spacer length). Peptide samples in the same buffer used in equilibrium sedimentation (1% C_8E_5, 200 mM NaCl, and 20 mM sodium phosphate, pH 7.0) were cross-linked at a range of peptide concentrations (0.2−8 mg/mL), cross-linker concentrations (100−500 μM), and cross-linking times (2 min−24 h). After quenching, the samples were subjected to MALDI-TOF mass spectrometry.

An example of the results from one set of experiments with 0.6 mg/mL peptide and 250 μM BS^3 during a 1 h time course is shown in Figure 5. The average molecular weight observed by equilibrium sedimentation at this peptide concentration corresponds to a dimer. Consistent with this finding, as shown in Figure 5B, the predominant cross-linked species corresponds to a dimer. Similar results were seen for all conditions when cross-linking was limited to 1 h or less. Higher order cross-linking could be observed if the reaction was allowed to proceed for 24 h, indicating that higher molecular weight species could have been observed in the mass spectrum if they were present.

The results of analytical ultracentrifugation of the MPZ-TM peptide in combination with chemical cross-linking and MALDI TOF mass spectrometry are consistent with preferential dimerization of the MPZ-TM peptide in detergent micelles. Although the inclusion of some possible tetramer is required to improve the goodness of fit to the equilibrium centrifugation results, all available evidence indicates that the primary, high-affinity interaction of the MPZ-TM peptide is a dimer.

Mapping the Dimeric Packing Interface by Alanine and Leucine Scanning. To identify residues important for mediating MPZ TM domain dimerization, we measured the effects of mutants on the TOXCAT assay. We introduced a Leu or

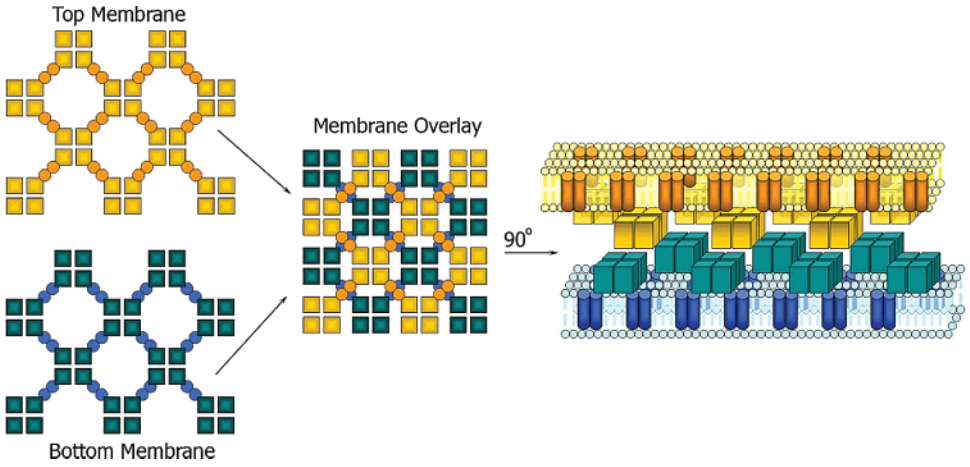

FIGURE 9: Possible model for construction of the myelin sheath. In the model, MPZ homodimerizes in the membrane via its 26-residue TM domain (represented as circles and cylinders), allowing the ECD (represented as squares and blocks) to participate in tetrameric bundles within the extracellular space. These tetramers would then radiate out from apposing membranes and intercalate in a "knobs in holes" configuration, adhering adjacent layers of the myelin sheath by forming a two-dimensional lattice. On the basis of this model, one can imagine how mutations within either domain could contribute to an overall destabilization of the quaternary structure of MPZ, resulting in disease.

Ala substitution at every position of the MPZ TM, unless the wild-type residue was already a Leu or Ala. In addition, both known disease-related mutations (G134R and G138R) were recreated.

Maltose complementation assays were first performed on each construct to verify expression in the proper orientation in the inner membrane. Figure 6 illustrates the results. For a negative control, a TOXCAT construct missing a TM domain was used. Positive controls for growth were TOXCAT constructs containing the TM domains of GpA and the GpA 83I mutant, which have already been shown to grow in maltose complementation assays (*22*).

Figure 7A illustrates the TOXCAT assay results for the mutant proteins. The mutants with the largest deleterious effects on dimerization (less than 60% MPZ WT) tend to be in the N-terminal two-thirds of the MPZ TM (G126L, V127A, G130A, G130L, A131L, G134L, G134R, G138A, and Gl38L), which includes an extended glycine zipper (G126, G130, G134, G138). Surprisingly, a number of mutants in the C-terminal third of the TM show significantly increased CAT activity, suggesting that these mutations might enhance dimerization (most notably L142A, F147L, Y148A, Y148L, and V149L). Western blots of whole-cell lysates indicated that all of the constructs were expressed at similar levels (data not shown).

The results of the TOXCAT assays for the N-terminal region are displayed on a helical wheel plot in Figure 7B. The mutations with most deleterious effects cluster on one side of the helical wheel. This surface appears to define the main interaction interface of the MPZ TM helix dimer.

Model for the Dimer. To build a possible model of the MPZ TM helix dimer, we utilized a simple packing algorithm that has proven effective for homo-oligomeric TM helical bundles. The algorithm finds a favorable packing arrangement subject to the symmetry constraints on a TM helix dimer. The resulting model is shown in Figure 8A. The putative packing interface involves the glycine zipper residues and, as is commonly observed in glycine packing interfaces, the helices adopt a right-handed packing angle (*37*).

As the model was built without knowledge of the TOXCAT assay results, the mutants provide an independent test of the model. As can be seen in Figure 8A, the key residues are found in the dimer interface. Correspondence with the model is further illustrated in Figure 8B, which shows a comparison of the mutant TOXCAT assay results and the Cα−Cα distances between helices. The correlation between the two is readily apparent, especially in the N-terminal two-thirds of the TM helix, which apparently comprises the main interaction surface of the putative dimer.

Disease-Related Mutations. Two mutations in the MPZ TM domain, G134R and G138R, are associated with two different hereditary diseases: Charcot−Marie−Tooth disease type 1B (*38*), and Dejerine−Sottas syndrome (*39*), respectively. We therefore sought to test the effect of both mutations on the ability to drive dimerization using the TOXCAT assay. G138R failed to insert into the membrane as judged by the maltose complementation assay (Figure 6). The G134R mutant did insert, but it showed severely diminished CAT activity (Figure 7A). These are intriguing results considering the relative severities and differing features of the two diseases; CMT1B is caused by the G134R mutation and is characterized by a late-onset phenotype with axonal degeneration, whereas DSS (caused by G138R) is a more severe, early-onset disease, characterized by extreme demyelination.

DISCUSSION

We have found that the TM domain of MPZ strongly drives oligomerization. We have mapped the oligomeric TM interface of MPZ in biological membranes, using alanine/leucine scanning of MPZ in the TOXCAT system. The interaction surface incorporates multiple, tandem GxxxG motifs, forming a glycine zipper known to be a common element in many homo-oligomeric transmembrane helix associations. A disease-causing mutation in the glycine zipper, G134R, strongly reduces oligomerization assessed by the TOXCAT assay, suggesting that TM oligomerization may be a key element of proper MPZ function.

The evidence is consistent with preferential formation of dimers by the MPZ TM domain. While the TM domain

peptide alone is prone to aggregation, the predominant form at lower concentrations is a dimer. Moreover, mutational mapping of the oligomerization interface in membranes shows no evidence for higher order oligomers. In particular, we built a three-dimensional model for a TM domain dimer that appears to explain all the deleterious mutations. If higher order oligomerization occurred, we might have expected the emergence of a clear second interface from the mutant analysis that is not occluded in the dimer.

A hypothetical model for extracellular domain (ECD) packing in the myelin sheath was previously proposed, based on the crystal packing observed in the crystal structure of the rat MPZ ECD (*17*), but this model cannot be obviously reconciled with our results. In the crystal structure, a sheet of tetramers pack against a second sheet of tetramers that is flipped 180° around an axis parallel to the first sheet. This arrangement suggests a mechanism for building the myelin sheath in which two membranes are brought together by interweaving ECD sheets (see ref *17*).

Our finding that the MPZ TM domain dimerizes is incompatible with the adhesion model based on crystal packing, however. In particular, the symmetry of the dimer does not match the symmetry *within* an ECD tetramer and the locations of the C-termini are too far apart to allow dimerization *between* tetramers in the model.

The combination of tetramer formation mediated by the ECD and dimers mediated by the TM domain suggests an alternative model illustrated in Figure 9. Dimers of tetramers would naturally form a two-dimensional lattice. The spacing between membranes is 46 Å (*40*, *41*, *42*), which would require interdigitation of the ECDs. As shown in Figure 9, the proposed lattice would leave holes into which the apposing tetramer knobs could insert, generating a cooperative assembly. We believe this model is consistent with the experimental evidence, including the variable reports of MPZ dimers and tetramers found in different organisms, but it remains highly speculative until more structural data have been gathered on myelin.

ACKNOWLEDGMENT

We thank Dr. Donald Engelman for providing the TOXCAT system and lab members for critical reading of the manuscript.

REFERENCES

1. Everly, J. L., Brady, R. O., and Quarles, R. H (1973) Evidence that the major protein in rat sciatic nerve myelin is a glycoprotein, *J. Neurochem. 21*, 329−334.
2. Lemke, G., and Axel, R. (1985) Isolation and sequence of a cDNA encoding the major structural protein of peripheral myelin, *Cell 40*, 501−508.
3. Lemke, G., Lamar, E., and Patterson, J. (1988) Isolation and analysis of the gene encoding peripheral myelin protein zero, *Neuron 1*, 73−83.
4. Doyle, J. P., and Colman, D. R. (1993) Glial-neuron interactions and the regulation of myelin formation. *Curr. Opin. Cell Biol. 5*, 779−785.
5. Kirschner, D. A., Martini, R., and Ganser, A. L. (1980) Compact myelin exists in the absence of basic protein in the shiverer mutant mouse, *Nature 283*, 207−210.
6. Saavedra, R. A., Fors, L., Aebersold, R. H., Arden, B., Horvath, S., Sanders, J., and Hood, L. (1989) The myelin proteins of the shark brain are similar to the myelin proteins of the peripheral nervous system, *J. Mol. Evol. 29*, 149−156.
7. Wells, C. A., Saavedra, R. A., Inouye, H., and Kirschner, D. A. (1993) Myelin P0-glycoprotein: Predicted structure and interactions of extracellular domain, *J. Neurochem. 61*, 1987−1995.
8. Hayasaka, K., Himoro, M., Sato, W., Takada, G., Uyemura, K., Shimizu, N., Bird, T. D., Conneally, P. M., and Chance, P. F. (1993) Charcot-Marie-Tooth neuropathy type 1B is associated with mutations of the myelin P0 gene, *Nat. Genet. 5*, 31−34.
9. Patel, P. I., and Lupski, J. R. (1994) Charcot-Marie-Tooth disease: a new paradigm for the mechanism of inherited disease, *Trends Genet. 10*, 128−133.
10. Warner, L. E., Hilz, M. J., Appel, S. H., Killian, J. M., Kolodny, E. H., Karpati, G., Carpenter, S., Watters, G. V., Wheeler, C., Witt, D., Bodell, A., Nelis, E., Van Broeckhoven, C., and Lupski, J. R. (1996) Clinical phenotypes of different MPZ (P0) mutations may include Charcot-Marie-Tooth type 1B, Dejerine-Sottas, and congenital hypomyelination, *Neuron 17*, 451−460.
11. Giese, K. P., Martini, R., Lemke, G., Soriano, P., and Schachner, M. (1992) Mouse P0 gene disruptiom leads to hypomyelination, abnormal expression of recognition molecules, and degeneration of myelin and axons, *Cell 71*, 565−576.
12. Kirschner, D. A., and Saavedra, R. A. (1994) Mutations in demyelinating peripheral neuropathies support molecular model of myelin P0-glycoprotein extracellular domain, *J. Neurosci. Res. 39*, 63−69.
13. Hasse, B., Bosse, F., Hanenberg, H., and Müller, H. W. (2004) Peripheral myelin protein 22 kDa and protein zero: domain specific trans-interactions, *Mol. Cell. Neurosci. 27*, 370−378.
14. Shy, M. E., Jani, A., Krajewski, K., Grandis, M., Lewis, R. A., Li, J., Shy, R. R., Balsamo, J., Lilien, J., Garbern, J. Y., and Kamholz, J. (2004) Phenotypic clustering in MPZ mutations, *Brain 127*, 371−384.
15. Lee, Y. C., Soong, B. W., Liu, Y. T., Lin, K. P., Kao, K. P., and Wu, Z. A. (2005) Median nerve motor conduction velocity is concordant with myelin protein zero gene mutation, *J. Neurol. 252*, 151−155.
16. Lai, C., Brow, M. A., Nave, K., Noronha, A. B., Quarles, R. H., Bloom, F. E., Milner, R. J., and Sutcliffe, J. G. (1987) Two forms of 1B236/myelin-associated glycoprotein, a cell adhesion molecule for post-natal neural development, are produced by alternative splicing, *Proc. Natl. Acad. Sci. U.S.A. 84*, 4337−4341.
17. Shapiro, L., Doyle, J. P., Hensley, P., Colman, D. R., and Hendrickson, W. A. (1996) Crystal structure of the extracellular domain from P0, the major structural protein of peripheral nerve myelin, *Neuron 17*, 435−449.
18. Inouye, H., Tsuruta, H., Sedzik, J., Uyemura, K., and Kirschner, D. A. (1999) Tetrameric assembly of full-sequence protein zero myelin glycoprotein by synchrotron X-ray scattering, *Biophys. J. 76*, 423−437.
19. Favereaux, A., Lagueny, A., Vital, A., Schmitter, J.-M., Chaignepain, S., Ferrer, X., Labatut-Cazabat, I., Vital, C., and Petry, K. G. (2003) Serum IgG antibodies to PO dimer and 35 kDa PO related protein in neuropathy associated with monoclonal gammopathy, *J. Neurol., Neurosurg. Psychiatry 74*, 1262−1266.
20. Thompson, A. J., Cronin, M. S., and Kirschner, D. A. (2002) Myelin protein zero exists as dimers and tetramers in native membranes of *Xenopus laevis* peripheral nerve, *J. Neurosci. Res. 67*, 766−771.
21. Kim, S., Jeon, T., Oberai, A., Yang, D., Schmidt, J. J., and Bowie, J. U. (2005) Transmembrane glycine zippers: Physiological and pathological roles in membrane proteins, *Proc. Natl. Acad. Sci. U.S.A. 102*, 14278−14283.
22. Russ, W. P., and Engelman, D. M. (1999) TOXCAT: A measure of transmembrane helix association in a biological membrane, *Proc. Natl. Acad. Sci. U.S.A. 96*, 863−868.
23. Sulistijo, E. S., Jaszewski, T. M., and MacKenzie, K. R. (2003) Sequence-specific dimerization of the transmembrane domain of the "BH3-only" protein BNIP3 in membranes and detergent, *J. Biol. Chem. 278*, 51959−51956.
24. Shaw, W. W. (1975) Chloramphenicol acetyl transferase from chloramphenicol-resistant bacteria, *Methods Enzymol. 43*, 737−755.
25. Schey, K. L., Papac, D. I., Knapp, D. R., and Crouch, R. K. (1992) Matrix-assisted laser desorption mass spectrometry of rhodopsin and bacteriorhodopsin, *Biophys. J. 63*, 1240−1243.
26. Melnyk, R. A., Partridge, A. W., Yip, J., Wu, Y., Goto, N. K., and Deber, C. M. (2003) Polar residue tagging of transmembrane peptides, *Biopolymers 71*, 675−685.

27. Sreerama, N., and Woody, R. W. (1993) A self-consistent method for the analysis of protein secondary structure from circular dichroism, *Anal. Biochem. 209*, 32−44.
28. Fleming, K. G., Ackerman, A. L., and Engelman, D. M. (1997) The effect of point mutations on the free energy of transmembrane α-helix dimerization, *J. Mol. Biol. 272*, 266−275.
29. Cohn, E. J., and Edsall, J. T. (1943) Density and apparent specific volume of proteins, in *Proteins, Amino Acids and Peptides as Ions and Dipolar Ions* (Cohn, E. J., and Edsall, J. T., Eds.) pp 370−381, Reinhold Publishing Corp., New York.
30. Laue, T. M., Shah, B. D., Ridgeway, T. M., and Pelletier, S. L. (1992) Computer-Aided Interpretation of Analytical Sedimentation Data for Proteins, in *Analytical Ultracentrifugation in Biochemistry and Polymer Science* (Harding, S.E., Rowe, A. J., and Horton, J. C., Eds.) pp 90−125, The Royal Society of Chemistry, Cambridge, U.K.
31. Kim, S., Chamberlain, A. K., and Bowie, J. U. (2003) A simple method for modeling transmembrane helix oligomers, *J. Mol. Biol. 329*, 831−840.
32. Kim, S., Chamberlain, A. K., and Bowie, J. U. (2004) Membrane channel structure of *Helicobacter pylori* vacuolating toxin: role of multiple GXXXG motifs in cylindrical channels, *Proc. Natl. Acad. Sci. U.S.A. 101*, 5988−5991.
33. Bower, M. J., Cohen, F. E., and Dunbrack, R. L., Jr. (1997) Prediction of protein side-chain rotamers from a backbone-dependent rotamer library: a new homology modeling tool, *J. Mol. Biol. 267*, 1268−1282.
34. Mendrola, J. M., Berger, M. B., King, M. C., and Lemmon, M. A. (2002) The single transmembrane domains of ErbB receptors self-associate in cell membranes, *J. Biol. Chem. 277*, 4704−4712.
35. Chin, C-N., Sachs, J. N., and Engelman, D. M. (2005) Transmembrane homodimerization of receptor-like protein tyrosine phosphatases, *FEBS Lett. 579*, 3855−3858.
36. Langosch, D., Brosig, B., Kolmar, H., and Fritz, H.-J. (1996) Dimerisation of the glycophorin A transmembrane segment in membranes probed with the ToxR transcription activator, *J. Mol. Biol. 263*, 525−530.
37. Walters, R. F.S., and DeGrado, W. F. (2006) Helix-packing motifs in membrane proteins, *Proc. Natl. Acad. Sci. U.S.A. 103*, 13658−13663.
38. Eggers, S. D., Keswani, S. C., Melli, G., and Cornblath, D. R. (2004) Clinical and genetic description of a family with Charcot-Marie-Tooth disease type 1B from a transmembrane MPZ mutation, *Muscle Nerve 29*, 867−869.
39. Simonati, A., Fabrizi, G. M., Taioli, F., Polo, A., Cerini, R., and Rizzuto, N. (2002) Dejerine-Sottas neuropathy with multiple nerve roots enlargement and hypomyelination associated with a missense mutation of the transmembrane domain of MPZ/P0, *J. Neurol. 249*, 1298−1302.
40. Kirschner, D. A., Inouye, H., Ganser, A. L., and Mann, V. (1989) Myelin membrane structure and composition correlated: a phylogenetic study, *J. Neurochem. 53*, 1599−1609.
41. Blaurock, A. E., Genter St Clair, M. B., and Graham, D. G. (1991) Membrane flow within the myelin sheath in IDPN neuropathy, *Neuropathol. Appl. Neurobiol. 17*, 309−321.
42. Kirschner, D. A., and Blaurock, A. E. (1992) Organization, phylogenetic variation, and dynamic transitions of myelin, in *Myelin: Biology and Chemistry* (Martinson, R. E., Ed) pp 3−78, CRC Press, Boca Raton, FL.

BI701066H